

Fluorine-plasma treated AlGaN/GaN high electronic mobility transistors under off-state overdrive stress

Dongyan Zhao(赵东艳), Yubo Wang(王于波), Yanning Chen(陈燕宁), Jin Shao(邵瑾), Zhen Fu(付振), Fang Liu(刘芳), Yanrong Cao(曹艳荣), Faqiang Zhao(赵法强), Mingchen Zhong(钟明琛), Yasong Zhang(张亚松), Maodan Ma(马毛旦), Hanghang Lv(吕航航), Zhiheng Wang(王志恒), Ling Lv(吕玲), Xuefeng Zheng(郑雪峰), and Xiaohua Ma(马晓华)

Citation: Chin. Phys. B, 2022, 31 (**11**): 117301. DOI: 10.1088/1674-1056/ac81a7

What follows is a list of articles you may be interested in

Improved device performance of recessed-gate AlGaN/GaN HEMTs by using *in-situ* N_2O radical treatment

Xinchuang Zhang(张新创), Mei Wu(武玫), Bin Hou(侯斌), Xuerui Niu(牛雪锐), Hao Lu(芦浩), Fuchun Jia(贾富春), Meng Zhang(张濛), Jiale Du(杜佳乐), Ling Yang(杨凌), Xiaohua Ma(马晓华), and Yue Hao(郝跃)

Chin. Phys. B, 2022, 31 (**5**): 057301. DOI: 10.1088/1674-1056/ac48fb

High power-added-efficiency AlGaN/GaN HEMTs fabricated by atomic level controlled etching

Xinchuang Zhang(张新创), Bin Hou(侯斌), Fuchun Jia(贾富春), Hao Lu(芦浩), Xuerui Niu(牛雪锐), Mei Wu(武玫), Meng Zhang(张濛), Jiale Du(杜佳乐), Ling Yang(杨凌), Xiaohua Ma(马晓华), and Yue Hao(郝跃)

Chin. Phys. B, 2022, 31 (**2**): 027301. DOI: 10.1088/1674-1056/ac1414

Protection of isolated and active regions in AlGaN/GaN HEMTs using selective laser annealing

Mingchen Hou(侯明辰), Gang Xie(谢刚), Qing Guo(郭清), and Kuang Sheng(盛况)

Chin. Phys. B, 2021, 30 (**9**): 097302. DOI: 10.1088/1674-1056/abf34c

Short-gate AlGaN/GaN high-electron mobility transistors with BGaN buffer

Tie-Cheng Han(韩铁成), Hong-Dong Zhao(赵红东), Xiao-Can Peng(彭晓灿)

Chin. Phys. B, 2019, 28 (**4**): 047302. DOI: 10.1088/1674-1056/28/4/047302

Theoretical analytic model for RESURF AlGaN/GaN HEMTs

Hao Wu(吴浩), Bao-Xing Duan(段宝兴), Luo-Yun Yang(杨珞云), Yin-Tang Yang(杨银堂)

Chin. Phys. B, 2019, 28 (**2**): 027302. DOI: 10.1088/1674-1056/28/2/027302

Fluorine-plasma treated AlGaN/GaN high electronic mobility transistors under off-state overdrive stress

Dongyan Zhao(赵东艳)[1], Yubo Wang(王于波)[1], Yanning Chen(陈燕宁)[1,2], Jin Shao(邵瑾)[1], Zhen Fu(付振)[2], Fang Liu(刘芳)[2], Yanrong Cao(曹艳荣)[3,4,†], Faqiang Zhao(赵法强)[1], Mingchen Zhong(钟明琛)[2], Yasong Zhang(张亚松)[3,‡], Maodan Ma(马毛旦)[3], Hanghang Lv(吕航航)[3], Zhiheng Wang(王志恒)[3], Ling Lv(吕玲)[4], Xuefeng Zheng(郑雪峰)[4], and Xiaohua Ma(马晓华)[4]

[1] *Beijing Engineering Research Center of High-reliability IC with Power Industrial Grade, Beijing Smart-Chip Microelectronics Technology Co., Ltd., Beijing* 100192, *China*

[2] *Beijing Chip Identification Technology Co., Ltd., Beijing* 102200, *China*

[3] *School of Electro-Mechanical Engineering, Xidian University, Xi'an* 710071, *China*

[4] *Key Lab of Wide Band-Gap Semiconductor Materials and Devices, Xidian University, Xi'an* 710071, *China*

(Received 6 May 2022; revised manuscript received 29 June 2022; accepted manuscript online 18 July 2022)

Influences of off-state overdrive stress on the fluorine-plasma treated AlGaN/GaN high-electronic mobility transistors (HEMTs) are experimentally investigated. It is observed that the reverse leakage current between the gate and source decreases after the off-state stress, whereas the current between the gate and drain increases. By analyzing those changes of the reverse currents based on the Frenkel–Poole model, we realize that the ionization of fluorine ions occurs during the off-state stress. Furthermore, threshold voltage degradation is also observed after the off-state stress, but the degradations of AlGaN/GaN HEMTs treated with different F-plasma RF powers are different. By comparing the differences between those devices, we find that the F-ions incorporated in the GaN buffer layer play an important role in averting degradation. Lastly, suggestions to obtain a more stable fluorine-plasma treated AlGaN/GaN HEMT are put forwarded.

Keywords: AlGaN/GaN HEMT, fluorine plasma treatment, off-state overdrive stress

PACS: 73.61.Ey, 73.40.Kp, 73.40.Qv **DOI:** 10.1088/1674-1056/ac81a7

1. Introduction

GaN and related alloys have shown greater promise in high-temperature, high-power and high-frequency applications compared to traditional semiconductor materials.[1–3] Owing to such excellent performance characteristics as high saturation current, high cutoff frequency, and large power handling capabilities, AlGaN/GaN high-electron mobility transistors (HEMTs) are promising candidates for next-generation microwave power amplifiers and high-voltage switches.[4–8] The conventional AlGaN/GaN HEMTs are the depletion-mode (D-mode) devices with a negative threshold voltage ($V_{\rm th}$). In practice, the enhancement-mode (E-mode) HEMTs provide a simplified solution for circuit designing and can combine with D-mode HEMTs to realize the integrated D/E-mode digital circuits. Fluorine-plasma (F-plasma) treatment is an effective approach to converting AlGaN/GaN HEMTs from D-mode to E-mode.[9,10] Because of the high electronegativity, the F atoms, which are incorporated in the AlGaN barrier layer and the GaN buffer layer, tend to capture free electrons and become negative fixed charges which will help to deplete the two-dimensional electron gas (2DEGs) and deliver a positive shift of $V_{\rm th}$.[11,12] The change of $V_{\rm th}$ is roughly linear with the power and treatment time of CF_4 plasma,[13] which means that the conditions of F-plasma treatment have a strong effect on the threshold voltage ($V_{\rm th}$) of the device. Therefore, F-plasma treated AlGaN/GaN HEMTs have great application prospects. However, when the F-plasma treated HEMT is biased under stress conditions, those F-ions are unstable, and they may diffuse or be ionized during thermal stress and overdrive stress,[14–17] resulting in degradation of device performance. Some works proposed that the high-energy electrons injected under the gate will collide with F-ions during the stress, causing the threshold voltage to move negatively.[18,19] Some works put forward that degradation of GaN HEMTs treated by F-plasma RF power is related to migration of F-ions under the overdrive stress, and the dynamic equilibrium of F-ions migration movement causes the degradation to be saturated gradually.[20] However, there are also some other works claimed that the degradation may be caused by the growing defects in the barrier layer during high field stress.[17,21] From the above discussion, though extensive research on F-plasma treated AlGaN/GaN HEMTs has been carried out over the last decade, the degradation mechanism under overdrive stress remains unclear. Therefore, it is essential to improve the physical understanding of the degradation mechanisms, and to put forward effective solutions to prevent those degradations or to fabricate more stable F-plasma treated devices for real applications.

[†]Corresponding author. E-mail: yrcao@mail.xidian.edu.cn

[‡]Corresponding author. E-mail: 568695351@qq.com

© 2022 Chinese Physical Society and IOP Publishing Ltd

In this paper, F-plasma treated AlGaN/GaN HEMTs dealt with different F-plasma RF powers are stressed under the off-state overdrive conditions. A study on the performance and parameter variation between the fresh devices and the stressed devices is carried out in detail. The impacts of different F-plasma RF powers on the parameter degradation of stressed F-plasma treated devices are investigated. Suggestions to obtain a more stable F-plasma treated AlGaN/GaN HEMT are put forwarded lastly, and we present a novel device which can reduce the degradation caused by the instability of F-ions.

2. Devices and experiments

Figure 1 shows the schematic diagram of the F-plasma treated HEMTs used in this study. The AlGaN/GaN heterostructure, which was grown on a (0001) sapphire substrate by metal-organic chemical vapor deposition (MOCVD), consists of a GaN nucleation layer, a 2-μm-thick unintentionally doped GaN buffer layer, and an unintentionally doped 20-nm-thick $Al_{0.3}Ga_{0.7}N$ barrier layer. Room-temperature Hall measurements show that the concentration and the electron mobility of the 2DEGs are 1.12×10^{13} cm^{-2} and 1615 cm^2/(V·s), respectively. Ohmic contacts were based on a Ti/Al/Ni/Au (22 nm/140 nm/55 nm/45 nm) metallic system, which were followed by thermal annealing in nitrogen at 830 °C for 30 s, yielding a contact resistance typically around 1.0 Ω·mm. The Ni/Au/Ni (45 nm/200 nm/20 nm) Schottky gate was realized by the electron-beam evaporation technology. The gate length and width of devices are 0.5 μm and 100 μm, respectively.

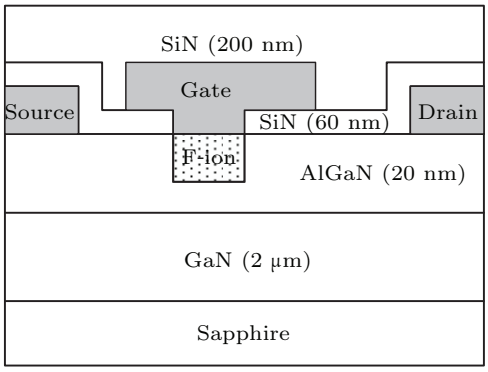


Fig. 1. Cross section of those F-plasma treatment HEMTs.

During the fabrication process of the F-plasma treated AlGaN/GaN HEMTs, before depositing the Schottky contact metal of the gate, the reactive ion etching (RIE) technology is utilized to perform the F-plasma treated process while CF_4 is used as the F source. The window at the Schottky contact area is the opening region while the other region is protected by the photoresist. Therefore, the F-ions can be implanted into the specific region. The power and time of RIE treatment determine the depth and amount of F-ions implanted. Obviously, the characteristics of the devices obtained under different conditions of F-plasma treatment are different. For comparison, HEMTs treated with different F-plasma RF powers are required. Three kinds of HEMTs, i.e., samples A, B and C, were fabricated with the same structure, except that the Schottky contact areas of different samples were treated with CF_4 plasma under different conditions. Table 1 shows the F-plasma treatment conditions of the three kinds of HEMTs. In addition, the F-plasma treated AlGaN/GaN Schottky barrier diodes were also fabricated using the same technology.

Table 1. Samples obtained under different conditions of F-plasma treatment.

Samples	Fluorine plasma treatment condition
A	without fluorine plasma treatment
B	80 W, 120 s
C	130 W, 120 s

Keithley 4200-SCS, a high precision semiconductor parameter analyzer, was used to complete the tests. Electrical parameters of fresh devices were measured to evaluate their initial properties. Then these devices were biased under the off-sate stress condition of $V_{G_STRESS} = -10$ V, $V_{D_STRESS} = 15$ V, $V_{S_STRESS} = 0$ V. The stress time of tests is 1000 s. In order to monitor the degradation of the devices, the stress was interrupted at regular intervals and electrical parameters were measured.

3. Results and discussion

3.1. Experiments details

The initial DC transfer and transconductance characteristics of all samples are presented in Fig. 2(a), and it is observed that all samples can work normally. In addition, the V_{th} of samples A (without F-plasma treatment), B (the F-plasma RF power and time are 80 W, 120 s) and C (the F-plasma RF power and time are 130 W, 120 s) are −2.81 V, −0.26 V, and 0.42 V, respectively, matching with the previous research which indicates that the threshold voltage of the F-plasma treated AlGaN/GaN HEMTs increases with the F-plasma RF power.[22] It is noteworthy that the V_{th} of sample C is positive, which indicates that sample C has been delivered to the E-mode. Figure 2(b) presents the output characteristic of sample C (E-mode HEMT).

In order to investigate the influence of the off-state stress on F-plasma treated HEMTs, samples are biased under the stress condition of $V_{G_STRESS} = -10$ V, $V_{D_STRESS} = 15$ V, $V_{S_STRESS} = 0$ V for 1000 s. With samples biased under the off-state stress condition, the gate channel is pinched off and strong electric fields are formed around the both ends of the gate. As shown in Fig. 3, the connections between the gate and source as well as between the gate and drain can be regarded as two F-plasma treated AlGaN/GaN Schottky barrier diodes

(SBD1 and SBD2). In addition, SBD1 is biased at the stress condition of $V_{\rm STRESS} = -10$ V, SBD2 is $V_{\rm STRESS} = -25$ V. While the characteristics of SBD1 are measured, the drain is floating. Similarly, the source is floating during measurement of the characteristics of SBD2.

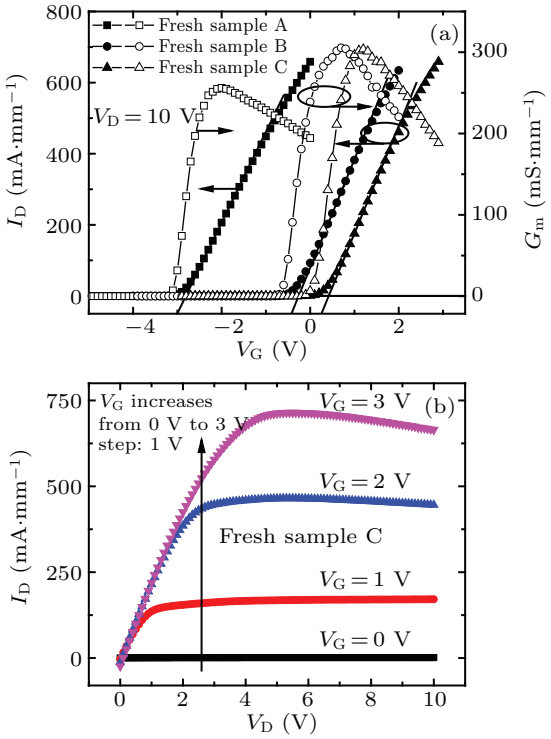


Fig. 2. (a) DC transfer and transconductance characteristics of fresh samples A, B, C. (b) Output characteristic of fresh sample C (E-mode HEMT).

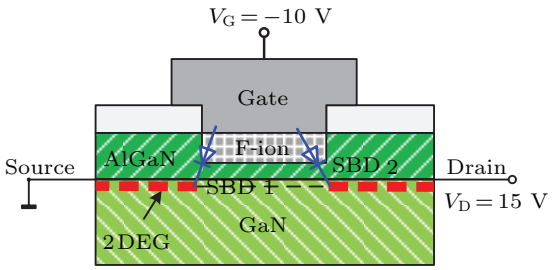


Fig. 3. The schematic of the device under the off-state stress.

3.2. The reverse currents of SBD1 and SBD2

The reverse *I*–*V* characteristics of SBD1 and SBD2 before and after the stress are shown in Figs. 4(a) and 4(b), respectively. It is obvious that the reverse leakage currents of SBD1 in samples B and C both decrease after the off-state stress, while the reverse leakage currents of SBD2 both increase. For the F-plasma treated SBDs, the transport mechanism of the reverse leakage current is supposed to be the Frenkel–Poole emission from the F-related deep level states into the dislocations related continuum states,[23] and the Frenkel–Poole emission current density is given by[24]

$$J = \frac{q\mu N_{\rm c}(N_{\rm d}-N_{\rm a})}{2N_{\rm a}} E_{\rm b} \exp\left[-\frac{q(\phi_{\rm t}-\sqrt{qE_{\rm b}/\pi\varepsilon_0\varepsilon_{\rm s}})}{rkT}\right], \quad (1)$$

where J is the emission current density, q is the charge of an electron, μ is the carrier mobility, $N_{\rm c}$ is the effective density of states in the conduction band, $N_{\rm d}$ is the density of donor sites, $N_{\rm a}$ is the density of acceptor sites, $\phi_{\rm t}$ is the barrier height for electron emission from a trap state, $E_{\rm b}$ is the electric field in the AlGaN barrier layer, $\varepsilon_{\rm s}$ is the high-frequency relative dielectric permittivity, ε is the permittivity of vacuum, T is thermodynamic temperature, k is Boltzmann's constant, and r is a parameter ranging from 1 to 2 depending on the position of the Fermi level. In the case of $n \ll N_{\rm a}$, $n \ll N_{\rm d}$ (n is the number of electrons in the conduction band), $r = 1$; in the case of $N_{\rm a} \ll n$, $N_{\rm a} \ll N_{\rm d}$, $r = 2$.

From Eq. (1), the liner relation between the $\ln(J/E_{\rm b})$ and $E_{\rm b}^{1/2}$ can be obtained as follows:

$$\begin{aligned}\ln\left(\frac{J}{E_{\rm b}}\right) &= \frac{q\sqrt{q/\pi\varepsilon_0\varepsilon_{\rm s}}}{rkT}\sqrt{E_{\rm b}} \\ &\quad + \ln\left(\frac{q\mu N_{\rm c}(N_{\rm d}-N_{\rm a})}{2N_{\rm a}}\right) - \frac{q\phi_{\rm t}}{rkT} \\ &\equiv A\sqrt{E_{\rm b}} + B, \quad (2)\end{aligned}$$

$$A = \frac{q\sqrt{q/\pi\varepsilon_0\varepsilon_{\rm s}}}{rkT}, \quad (3)$$

$$B = \ln\left(\frac{q\mu N_{\rm c}(N_{\rm d}-N_{\rm a})}{2N_{\rm a}}\right) - \frac{q\phi_{\rm t}}{rkT}. \quad (4)$$

The plots of $\ln(J/E_{\rm b})$ versus $E_{\rm b}^{1/2}$ for both SBD1 and SBD2 of samples B and C before and after stress are shown in Figs. 4(c)–4(f), respectively. Experimental data of $\ln(J/E_{\rm b})$ versus $E_{\rm b}^{1/2}$ are liner fitted, demonstrating that Frenkel–Poole emission is the transport mechanism of reverse leakage current in both fresh and stressed samples (including SBD1 and SBD2). However, the slopes (A) and intercepts (B) of SBD1 and SBD2 both changed after the off-state stress. For SBD1 of sample B, the slope increases from 0.00222 to 0.00426, and the intercept decreases from −21.60 to −23.69. For SBD2 of sample B, the slope increases from 0.00126 to 0.00210, the intercept decreases from −22.75 to −22.96. For SBD1 of sample C, the slope increases from 0.00358 to 0.00537, and the intercept decreases from −22.15 to −23.04. For SBD2 of sample B, the slope increases from 0.00338 to 0.00401, the intercept decreases from −22.62 to −22.67. Obviously, for both samples B and C before and after the off-state stress, the variation range of the slope and intercept in SBD2 are smaller than those in SBD1, which results in the different changes of the reverses leakage current in stressed SBD1 and SBD2. Moreover, the Frenkel–Poole model, in which the compensation effects of donor and acceptor sites to the Frenkel–Poole emission are considered,[24,25] can be used to further analyze those variations of the slope and intercept.

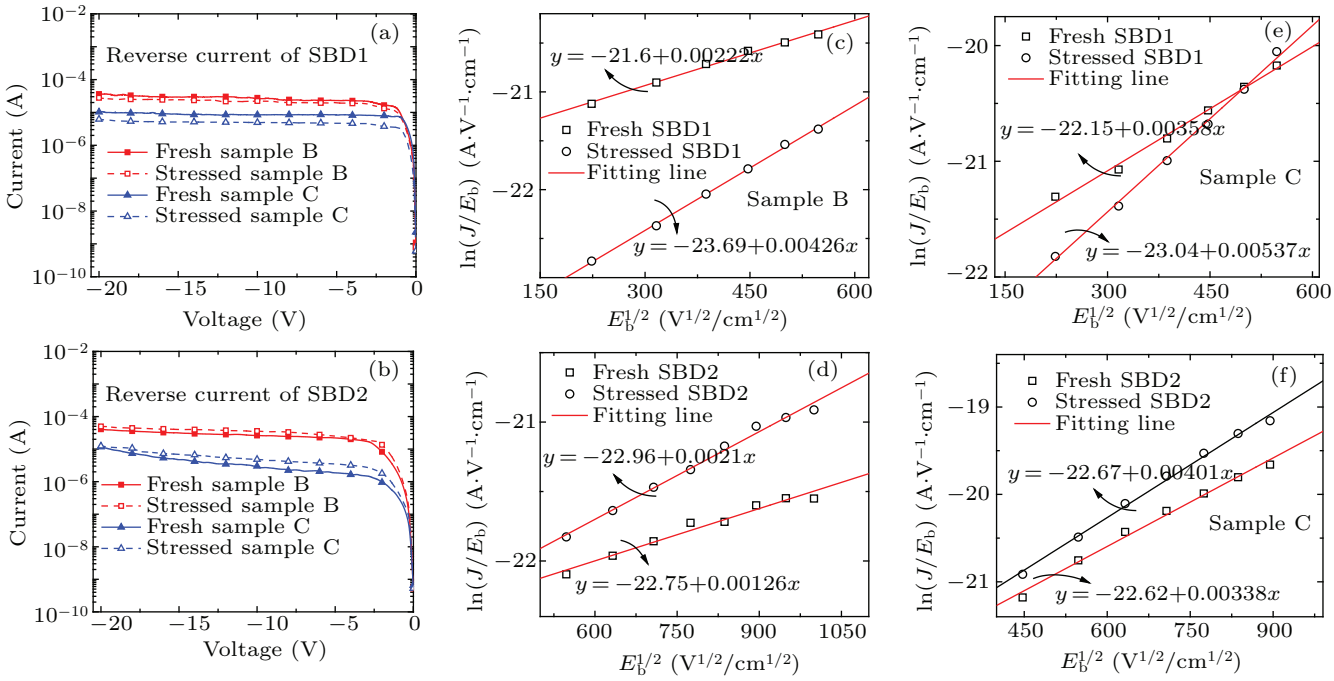


Fig. 4. The reverse *I*–*V* characteristics of (a) SBD1 and (b) SBD2 before and after stress. The plots of $\ln(J/E_b)$ versus $E_b^{1/2}$ for both (c) SBD1 and (d) SBD2 of sample B before and after stress. The plots of $\ln(J/E_b)$ versus $E_b^{1/2}$ for both (e) SBD1 and (f) SBD2 of sample C before and after stress.

3.3. The ionization of F-ions effect on SBD1

With devices biased under the reverse voltage stress, a high electric field is formed. Many gate electrons are injected into the AlGaN barrier and are accelerated by this electric field. When exposed to the negatively charged F-ions, those electrons, which have got huge kinetic energy, can ionize the F-ions.[26] The stable Ga–F bonds are formed during the process of the ionization of F-ions.[15] With the Ga-F bonds occupied some gallium atoms, some nitrogen atoms cannot form enough bonds with the gallium atoms to become saturated, causing the increase of the unsaturated nitrogen. The unsaturated nitrogen atoms are mainly acting as acceptors of electrons in the crystal, indicating that the N_a increases after the stress. As the N_a increases, the relationship among n, N_a and N_d gets closer to the case of $n \ll N_a$, $n \ll N_d$, which indicates that the value of r gets closer to 1, meaning that the value of r decreases after the stress. According to Eqs. (3) and (4), changes of N_a and r result in the decrease of the intercept (B) and the increase of the slope (A), which agree with the above experimental data of SBD1 shown in Figs. 4(c) and 4(e).

Furthermore, because of the high electric field, many traps are generated at the gate-metal/AlGaN interface. Those new traps can capture electrons after the stress and lead to Fermi-level pinning with a lower level at the Gate metal/AlGaN interface,[27] which will increase the barrier height ϕ_t of FP emission and result in the reduction of the reverse leakage current in SBD1 (as shown in Fig. 4(a)). In addition, the ionization of the negatively charged F-ions weakens the depletion effect on 2DEGs, leading to the negative shift of the threshold voltage. In order to verify the above analysis, the fluorine plasma treated AlGaN/GaN SBDs are stressed under the condition of $V_{G_STRESS} = -10$ V for 1000 s. Figure 5 shows the *C*–*V* characteristics of those devices. It is seen that the threshold voltage decreases with the increasing stress time, consistent with the above analysis. Thus, some F-ions in the SBD1 were ionized during the off-state stress.

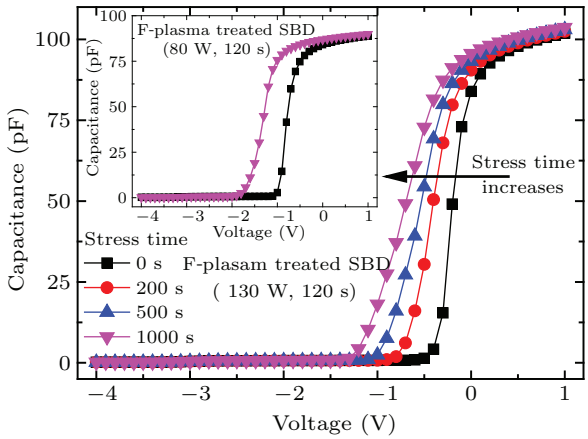


Fig. 5. The *C*–*V* characteristics of fluorine plasma treated AlGaN/GaN SBDs under the stress condition of $V_{G_STRESS} = -10$ V at different stress times. The F-plasma treated AlGaN/GaN SBD is circular, and the diameter of its anode is 130 μm; the distance between anode and cathode is 30 μm.

From the above analysis of SBD1, it can be concluded that some F-ions in the devices can be ionized during the high stress, which results in the decreased intercept (B) and the increased slope (A) of the SBD1 at last. Furthermore, the *C*–*V* characteristics can prove the analysis.

3.4. Synergistic effects of F-ions ionization and inverse piezoelectric effect on SBD2

The stress condition of $V_{G_STRESS} = -25$ V for SBD2 is larger than the critical voltage (V_C), over which an AlGaN/GaN HEMT will experience the inverse piezoelectric effect (the typical value of V_C is about -20 V[28]). Thus, the inverse piezoelectric effect induced lattice defects may be formed in the AlGaN barrier layer after the stress. Those lattice defects are as donors of electrons in the crystal,[29] indicating the increase of the N_d and the consequent increase of the n. As n and N_d both increase, the relationship among n, N_a and N_d gets more close to the case of $N_a \ll n$, $N_a \ll N_d$, which indicates that the value of r gets more close to 2, meaning that the value of r increases after the stress. According to Eqs. (3) and (4), the increases of the r and N_d result in the decrease of slope (A) and the increase of intercept (B), respectively. However, the transport mechanism of the leakage current in SBD2 is still the Frenkel–Poole emission, and the ionization of the F-ions also occurs during the stress, which still results in the increase of slope (A) and the decrease of intercept (B), respectively. Those two effects will counteract each other, as shown in Figs. 4(d) and 4(f). At last, the increase of the slope (A) and the decrease of intercept (B) become weak in SBD2 by the synergistic effects of ionization of F-ions and inverse piezoelectric effect.

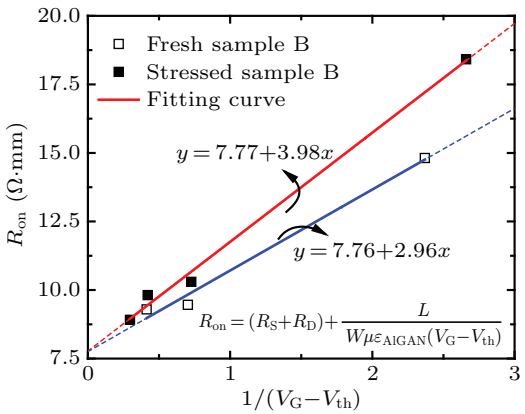


Fig. 6. The channel resistance R_{on} of the sample B before and after the off-state stress.

In addition, those lattice defects may increase the trap-assisted-tunneling (TAT) current. Also, they may overlap with each other and form a leakage path, resulting in the increase of the reverse leakage current (as shown in Fig. 4(b)). Moreover, the lattice defects, produced by the inverse piezoelectric effect can increase the scattering of conduction electrons, which will result in the increase of the channel resistance. In order to proof the inverse piezoelectric effect, the channel resistances R_{on} of sample B before and after the off-state stress are extracted from the output characteristic and are presented in Fig. 6. It shows that R_{on} increases after the stress, which results from the formation of the lattice defects at the AlGaN/GaN interface and agrees with the above analysis.

From the above analysis of SBD2, we can obtain that F-ions ionization and the inverse piezoelectric effect can both occur near the drain under the high off-state stress, and the synergistic effect weakens the increase of the slope (A) and the decrease of intercept (B) in SBD2. The increased R_{on} approves the conclusion.

3.5. Effect of F-ions on V_{th}

According to the above analyses, the ionization of the negatively charged F-ions arises around the both ends of the gate (SBD1 and SBD2) during the overdrive stress, which weakens the depletion effect of F-ions on 2DEGs, leading to the increase of the 2DEG density and the consequent negative shift of threshold voltage. However, as shown in Fig. 7, V_{th}'s of samples B and C have different degradations under the same stress condition. In detail, V_{th} of sample B degrades under the off-state stress and the degradation becomes serious as the stress time increases, while V_{th} of sample C degrades much smaller. There are three reasons for this phenomenon.

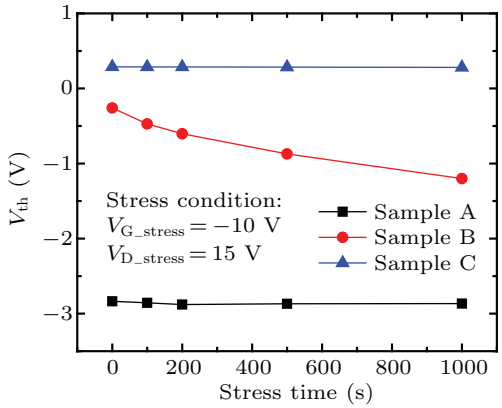


Fig. 7. Stress time dependence of V_{th} of samples A (square), B (circle) and C (triangle) under the off-state stress.

(i) The amount of injected electrons from the gate.

During the off-state stress, the ionization of the F-ions in AlGaN is caused by the injected gate electrons, and the quantity of the ionized F-ions is related to the amount of injected electrons. Therefore, the degradation of V_{th} shows strong dependence on the injected electron density.[16,26] According to Figs. 4(a) and 4(b), the reverse leakage currents of both SBD1 and SBD2 in sample C are much smaller than those in sample B, which means that the injected electrons from the gate in sample C are much less than those in sample B. Consequently, the quantity of the ionized F-ions in sample C is much smaller than that in sample B, and the V_{th} degradation of sample C is not pronounced.

(ii) The depth of F-ions in the AlGaN barrier layer.

The depth of F-ions implantation in the AlGaN barrier layer increases with the increase of the F-plasma RF power.

The ionization of the F-ions arises in the AlGaN barrier layer around the both ends of the gate (SBD1 and SBD2). If the off-state stress time is long enough, as shown in Fig. 8, the F-ions, which exist in the two triangle regions (SBD1 and SBD2), will be ionized after the stress, while the others will maintain mostly. The deeper the F-ions stay in the AlGaN layer, the more the F-ions will maintain after the off-state stress. Thus, the maintained F-ions in sample C treated with higher F-plasma RF power (130 W) are more than those in sample B treated with lower F-plasma RF power (80 W), which leads to the larger V_{th} degradation in sample B while smaller V_{th} degradation in sample C.

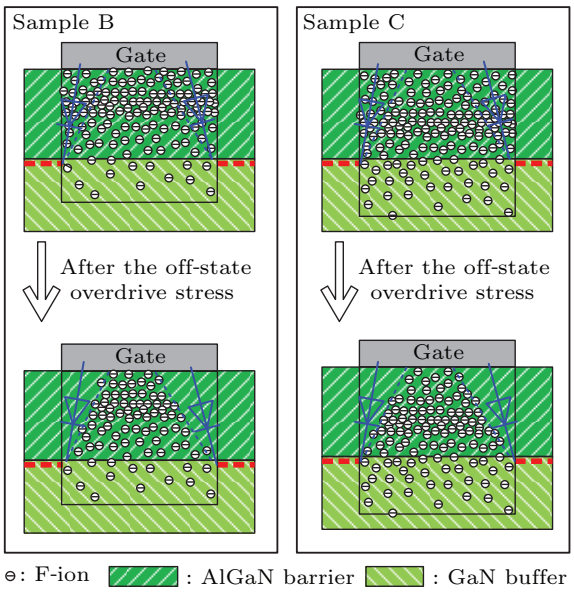


Fig. 8. The schematic of the F-ions distribution in fresh and stressed samples B (80 W) and C (130 W).

(iii) F-ions located at the GaN buffer layer.

The F-ions, which stay in the top layer of the GaN buffer layer, also play an important role in the depletion effect of the 2DEG. They can deplete the 2DEG and deliver a positive shift of V_{th}, too. TCAD simulation is employed and the structure parameters are the same for the devices used in the experiments, such as a 2-μm-thick GaN buffer layer, an unintentionally doped 20-nm-thick $Al_{0.3}Ga_{0.7}N$ barrier layer, 0.5 μm gate length and 100 μm gate width. Under the off-state overdrive stress condition ($V_G = -10$ V, $V_D = 15$ V, $V_S = 0$ V), the gate region electric field in the AlGaN barrier layer is stronger than that in the GaN buffer layer as shown in Fig. 9, which means that F-ions in the GaN buffer layer can avoid being influenced by the overdrive stress. For sample C, as shown in Fig. 8, because of the larger plasma treatment power, more F-ions stay in the GaN buffer layer and more F-ions retain after the off-state overdrive stress. Thus, the overdrive stress has a smaller influence on the V_{th} of sample C. Our previous work also shows that, during the reverse gate step-stress, the V_{th} of thin barrier F-plasma treated HEMTs are much more stable than that of the devices with a thicker barrier layer (those two kinds of devices are treated with the same CF_4 plasma RF power),[30] which may be caused by the F-ions which are incorporated in the GaN buffer layer.

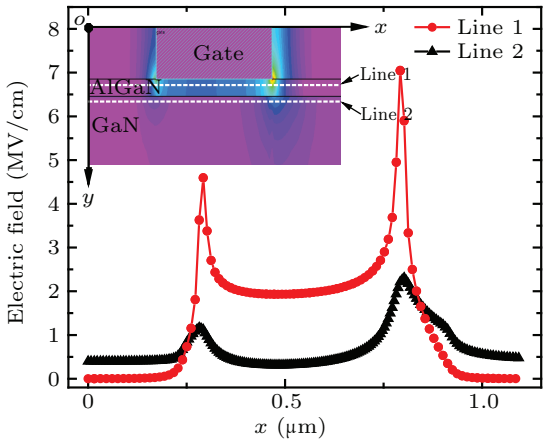


Fig. 9. Extracted electric field intensity distribution of lines 1 and 2 in AlGaN/GaN HEMT under off-state stressing condition, lines 1 and 2 are located respectively in the AlGaN barrier layer and in the GaN buffer layer. Inset: contour plot of electric field round the gate. The simulation is carried out with the TCAD simulator Silvaco Atlas, and the V_D is set at 15 V, V_G is set at −10 V and V_S is set at 0 V.

3.6. Methods to improve the stability of F-plasma treated devices

Combining with the above analyses and explanations, we can realize that the unreliable performance of F-plasma treated AlGaN/GaN HEMTs under off-state overdrive stress is mainly caused by the ionization of the negatively charged F-ions. The degree of V_{th} degradation is related to the quantity of the ionized F-ions. For sample C, most of the negatively charged F-ions are retained, resulting in the negligible V_{th} degradation.

Furthermore, as the ionization of the negatively charged F-ions is caused by the high electric field in the gate region, there are two ways to improve the stability and reliability of F-plasma treated devices: optimizing the distribution of electric field and changing the location of implanted F-ions. The gate-field-plate and dual-gate structure can be used to optimize the distribution of electric field around the gate region of F-plasma treated HEMTs.[14] Noticeably, before applications, it is necessary to do much work such as simulation of those structures and exploration of the optimal structural parameters, which will take a long time. Since the electric field of overdrive stress in the GaN buffer layer is weak and it has little influence on the F-ions incorporated in the GaN buffer layer, more stable F-plasma treated devices can be obtained when we focus on only implanting F-ions into the GaN buffer layer. One of these ideal stable F-plasma treated AlGaN/GaN HEMTs is shown in Fig. 10. TACD simulation shows that a smaller number of F-ions can convert the D-mode HEMTs into E-mode in this novel structure than that in the normal structure. The research on the manufacturing process for this structure is ongoing.

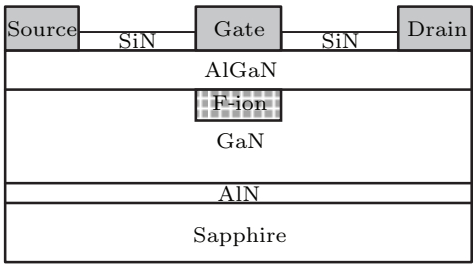


Fig. 10. An ideal stable F-plasma treated HEMT. F-ions only incorporated in the GaN buffer layer.

4. Conclusions

In summary, we have investigated the influences of the off-state overdrive stress on the F-plasma treated AlGaN/GaN HEMTs. After the off-state stress, the reverse leakage current between gate and source, as well as that between gate and drain, changes. The Frenkel–Poole model is carried out to analyze those changes of the reverse current and it suggests that the variation of the gate-source leakage current is mainly caused by the ionization of the F-ions, and that of the gate-drain leakage current is caused by the synergistic effects of the ionization of F-ions and inverse piezoelectric effect. The *C*–*V* characteristics and extracted channel resistances both bring a good agreement on those analyses. Furthermore, the reasons for different $V_{\rm th}$ degradations of HEMTs treated by different powers of F-plasma are discussed too. It is indicated that the F-ions incorporated in the GaN buffer layer can play an important role in averting degradation. Lastly, suggestions to obtain a more stable fluorine-plasma treated AlGaN/GaN HEMT are put forward, and a novel structure is also suggested.

Acknowledgements

Project supported by the Laboratory Open Fund of Beijing Smart-Chip Microelectronics Technology Co., Ltd and the National Natural Science Foundation of China (Grant Nos. 11690042 and 12035019), the National Major Scientific Research Instrument Projects (Grant No. 61727804), and the Natural Science Foundation of Shaanxi Province, China (Grant No. 2022-JM-386).

References

[1] Buniatyan V V and Aroutiounian V M 2007 *J. Phys. D: Appl. Phys.* **40** 6355
[2] Lian G 2020 *7th International Forum on Electrical Engineering and Automation (IFEEA)*, September 25–27, 2020, Hefei, China, pp. 149–152
[3] Perkins S, Arvanitopoulos A, Gyftakis K N and Lophitis N 2018 *IEEE 1st Workshop on Wide Bandgap Power Devices and Applications in Asia (WiPDA Asia)*, May 16–18, 2018, Xi'an, China, pp. 174–178
[4] Cai Y, Zhou Y, Chen K J and Lau K M 2005 *IEEE Electron Device Lett.* **26** 435
[5] Wang Y, Hu S D, Guo J W, Wu H, Liu T and Jiang J 2022 *IEEE J. Electron Devices Soc.* **10** 197
[6] Albahrani S A, Heuken L, Schwantuschke D, Gneiting T, Burghartz J N and Khandelwal S 2020 *IEEE Trans. Electron Devices* **67** 455
[7] Yadav Y K, Upadhyay B B, Meer M, Bhardwaj N, Ganguly S and Saha D 2019 *IEEE Electron Device Lett.* **40** 67
[8] Kobayashi K W and Kumar V 2021 *IEEE Microw Wirel Compon. Lett.* **31** 885
[9] Cai Y, Zhou Y, Lau K M and Chen K J 2006 *IEEE Trans. Electron Devices* **53** 2207
[10] Wu C H, Han P C, Luc Q H, Hsu C Y, Hsieh T E, Wang H C, Lin Y K, Chang P C, Lin Y C and Chang E Y 2018 *IEEE J. Electron Devices Soc.* **6** 893
[11] Chen K J, Yuan L, Wang M J, Chen H, Huang S, Zhou Q, Zhou C, Li B K and Wang J N 2011 *IEEE International Electron Devices Meeting*, December 5–7, 2011, Washington, DC, USA, pp. 19.4.1–19.4.4
[12] Mao L F 2019 *ECS J. Solid State Sci. Technol.* **8** 472
[13] Yong C, Zhou Y, Chen K J and Lau K M 2005 *IEEE Electron Device Lett.* **26** 435
[14] Wang M J, Yuan L, Chen K J, Xu F J and Shen B 2009 *J. Appl. Phys.* **105** 083519
[15] Ma C, Chen H, Zhou C, Huang S, Yuan L, Roberts J and Chen K J 2011 *J. Appl. Phys.* **110** 114514
[16] Yi C W, Wang R N, Huang W, Tang W C W, Lau K M and Chen K J 2007 *IEEE International Electron Devices Meeting*, December 10–12, 2007, Washington, DC, USA, pp. 389–392
[17] Albany F, Curutchet A, Labat N, Lecourt F, Walasiak E, Maher H, Cordier Y, Defrance N and Malbert N 2021 *IEEE 15th European Microwave Integrated Circuits Conference (EuMIC)*, January 10–15, 2021, Utrecht, Netherlands, pp. 237–240
[18] Yang L, Hou B, Mi M H, Zhu J J, Zhang M, Zhu Q, He Y L, Chen L X, Zhou X W, Ma X H and Hao Y 2017 *IEEE International Reliability Physics Symposium (IRPS)*, April 2–6, 2017, Monterey, CA, USA, pp. WB-2.1–WB-2.4
[19] Ma C Y, Chen H W, Zhou C H, Huang S, Yuan L, Roberts J, Kevin and Chen J 2011 *J. Appl. Phys* **110** 114514
[20] Yang L, Zhou X W, Ma X H, Lv L, Cao Y R, Zhang J C and Hao Y 2017 *Chin. Phys. B* **26** 017304
[21] Sun W W, Zheng X F, Fan S, Wang C, Du M, Zhang K and Chen W W 2015 *Chin. Phys. B* **24** 017303
[22] Quan S, Hao Y, Ma X H, Xie Y B and Ma J G 2009 *J. Semiconduct.* **30** 124002
[23] Ha W J, Chhajed S, Oh S J, Hwang S, Kim J K, Lee J H and Kim K S 2012 *Appl. Phys. Lett.* **100** 132104
[24] Yeargan J R and Taylor H L 1968 *J. Appl. Phys.* **39** 5600
[25] Ren J, Mou W J, Zhao L, Yan D W, Yu Z G, Yang G F, Xiao S Q and Gu X F 2017 *IEEE Trans. Electron Devices* **64** 407
[26] Zheng X F, Chen A S, Zhang H, Wang X H, Wang Y Z, Hua N, Chen K, Wang M S, Zhang Q Y, Ma X H and Hao Y 2020 *IEEE International Symposium on the Physical and Failure Analysis of Integrated Circuits (IPFA)*, July 20–23, 2020, Singapore, pp. 1–4
[27] Zhang Y S, Cao Y R, Li P, Dai F, Zhu Q, Lv L, Ma X H and Hao Y 2016 *IEEE 13th IEEE International Conference on Solid-State and Integrated Circuit Technology (ICSICT)*, October 25–28, 2016, Hangzhou, China, pp. 1035–1037
[28] Joh J and Alamo J J A 2006 *IEEE International Electron Devices Meeting*, December 11–13, 2006, San Francisco, CA, USA, pp 1–4
[29] Ren J, Yan D W and Gu X F 2013 *Acta Phys. Sin.* **62** 157202 (in Chinese)
[30] Ma X H, Yu H Y, Quan S, Yang L Y, Pan C Y, Yang L, Wang H, Zhang J C and Hao Y 2011 *Chin. Phys. B* **20** 027303